Journal of Visualization, Vol. 3, No. 2 (2000) 165-173

A Comparison of 2D and 3D PIV Measurements in an Oblique Jet

Abe, M.*1, Longmire, E. K.*2, Hishida, K.*1 and Maeda, M.*1

*1 Dept. of System Design Engineering, Keio University, 3-14-1 Hiyoshi, Kohoku-ku, Yokohama 223-8522, Japan.
*2 Dept. of Aerospace Engineering & Mechanics, University of Minnesota, 110 Union St., SE, Minneapolis, MN 55455, USA.

Received 21 January 2000.
Revised 8 May 2000.

***Abstract*:** A stereo PIV (SPIV) acquisition and analysis system was developed to measure three velocity components in planar flow fields. The analysis software is based on a third order mapping function method. The system was calibrated by imaging a square grid in three measurement planes with two Kodak Megaplus cameras oriented at 30° to the bisector between them. The camera images were dewarped into real coordinates by employing a set of transform matrices computed for each calibration plane. Bias and rms errors were determined by comparing displacements measured directly with displacements estimated from the dewarping and recombination algorithm. The bias errors in the directions parallel with the measurement plane were negligible while the bias in the z direction was about 0.6 pixel. The rms errors, 0.2-0.3 pixels, were largest in the z direction. These errors were thought to result from limitations in the calibration method. The SPIV system was tested in a two-dimensional oblique jet with Reynolds number of 1800. The three dimensional results were taken in a vertical (x, y) plane parallel with the jet span. The SPIV results were compared with LDV data and two-dimensional PIV data obtained in a vertical (y, z) plane of the same jet. The SPIV measurements yielded accurate values for the in-plane mean and rms velocity components. The measured out-of-plane mean component was underestimated due to the bias error mentioned above. The rms component was accurate in part of the field but overestimated in another part due to local variations in rms error. It is expected that in the future, the out-of-plane errors can be minimized by improving the calibration and transformation procedures.

***Keywords*:** Stereo PIV, inclined jet, LDV, measurement uncertainty.

1. Introduction

A stereoscopic PIV (SPIV) system is able to measure all three velocity components within small zones of a planar domain. Two types of implementation for SPIV have been reported. A 'non-calibration method' was demonstrated by Prasad and Adrian (1993). The method employs input parameters specific to the particular experiment, such as the refractive indices of fluid and container and measured dimensions between cameras and the 'image' region. The method also employs imaging optics with strict specifications (minimal aberration) to reconstruct three-component vectors without calibration. In contrast, Willert (1997) and Soloff, Adrian, and Liu (1997) discuss 'mapping function methods' that determine the mapping functions by in situ calibration. The mapping functions determined by this method are contained within matrices that transform the pixel coordinate systems aligned with the cameras into a real coordinate system aligned with the image plane. In this case, quantities such as refractive index need not be measured precisely, and optical aberrations do not introduce systematic errors.

In this paper, we describe a 'mapping function' SPIV system developed at Keio University. The mapping algorithms were calibrated and assessed by comparing with direct measurements of displacement. Then, the system was tested in an experiment with a steady mean cross flow. The SPIV results were compared with results from LDV and from a standard two-dimensional PIV method oriented perpendicular to the stereo measurement plane. The long-term objective of the work is to minimize uncertainty in all components in order to produce a viable system for the measurement of three-dimensional turbulent flows. In the following sections the system development, testing, application, and performance are described. Portions of this paper appeared in Abe et al. (1999).

2. Experimental Technique

2.1 Image Reconstruction Rethod and Recombination Procedure

The analysis software, which is based on a third-order mapping function method similar to the second-order strategy of Willert (1997), is described in detail in Abe (1999). In this case, the mapping function is represented by the matrix $\boldsymbol{A}$ in the following expression:

$\boldsymbol{x} = \boldsymbol{XA}$, or

$$\begin{bmatrix} x_1 & y_1 \\ x_2 & y_2 \\ \vdots & \vdots \\ \vdots & \vdots \\ x_n & y_n \end{bmatrix} = \begin{bmatrix} 1 & X_1 & X_1^2 & X_1^3 & X_1Y_1 & \cdots & X_1^3Y_1^3 & Y_1 & Y_1^2 & Y_1^3 \\ 1 & X_2 & X_2^2 & X_2^3 & X_2Y_2 & \cdots & X_2^3Y_2^3 & Y_2 & Y_2^2 & Y_2^3 \\ \vdots & \vdots & & & & \ddots & & & \vdots & \\ \vdots & \vdots & & & & \ddots & & & \vdots & \\ 1 & X_n & X_n^2 & X_n^3 & X_nY_n & \cdots & X_n^3Y_n^3 & Y_n & Y_n^2 & Y_n^3 \end{bmatrix} \begin{bmatrix} a_1 & b_1 \\ a_2 & b_2 \\ \vdots & \vdots \\ a_{16} & b_{16} \end{bmatrix}$$

In the equation above, $\boldsymbol{x}$ and $\boldsymbol{X}$ represent matrices describing n positions in real and pixel coordinates respectively. The elements of $\boldsymbol{x}$ and $\boldsymbol{X}$ are determined in the calibration process. The transform matrix $\boldsymbol{A}$ is determined using a linear least squares method:

$$\boldsymbol{A} = (\boldsymbol{x}^T\boldsymbol{X})^{-1}\boldsymbol{X}^T\boldsymbol{x},$$

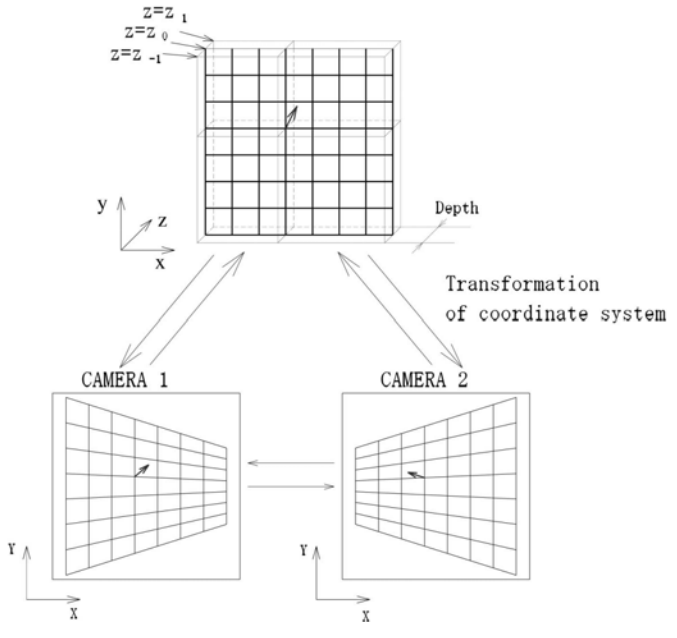

Fig. 1. Transformation between pixel and real coordinate planes.

where $\boldsymbol{x}$ and $\boldsymbol{X}$ are 'over determined' such that $n > 16$. The transform matrix $\boldsymbol{A}$ makes possible warping between a particular plane in real coordinates and a plane in pixel coordinates. In the system developed at Keio, a total of six transform matrices (three are redundant) are calculated for a given calibration plane at a specific z position. Figure 1 depicts the pixel and coordinate planes as well as the coordinate system relevant to the SPIV set up. Referring to the figure, the six coordinate transforms represent Camera 1 to Real, Camera 1 to Camera 2, Camera 2 to Real, and the three inverses. The z direction is normal to the measurement plane, while the x and y directions are parallel to the measurement plane. The x direction is defined parallel with the plane of the two cameras used, while the y direction is normal. In the experiments described below, a total of three calibration planes were used to compute 18 transform matrices.

The transform matrices generated by calibration are employed to reconstruct three-component displacement vectors from pairs of two-component vectors recorded in the two cameras. For a given displacement vector recorded in a camera plane, the tail is mapped to the center calibration plane (z_0), while the head is mapped to points in the z_{-1} and z_1 planes. This process is illustrated in Fig. 2. Note that the vector sizes are exaggerated in the figure. In practice, the vectors would lie entirely within the thickness of the laser sheet. Ideally, the pairs of points in the z_{-1} and z_7 planes determine two lines that intersect at the head of the 'real' displacement vector. In most cases, the two lines do not intersect due to uncertainties in computing the original two-component vectors. For this reason, a least squares method is employed to determine the position of the vector head. The method effectively calculates the midpoint of the minimum length segment connecting the two projection lines.

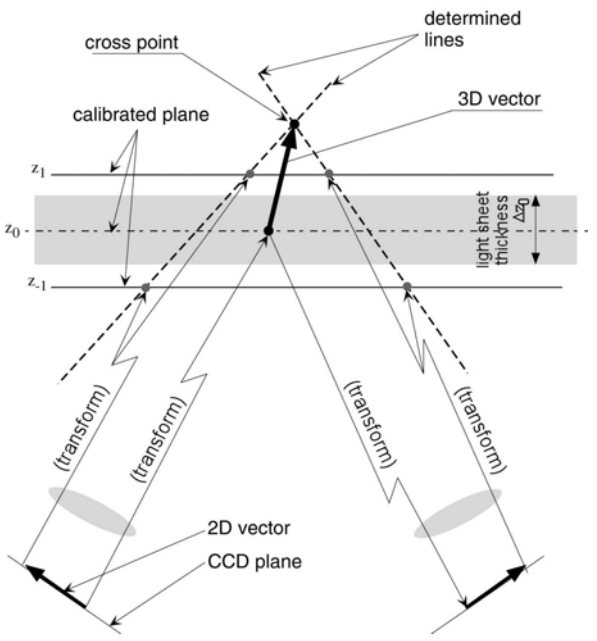

Fig. 2. Recombination procedure to form three-component vectors.

2.2 Moving Plate Experiment

The transformation and recombination software was tested by measuring displacements of a custom calibration plate covered with a square grid. The grid was displaced by micrometers attached to a traversing mechanism. (see Fig. 3). For this test, three calibration planes, spaced 3.5 mm apart, were used to obtain the transform matrices. Based on the 16×16 grid intersections used as calibration locations, the value of n in the $\boldsymbol{x}$ and $\boldsymbol{X}$ matrices was 256. The uncertainty in actual plate position was estimated as 10 microns.

The plate was imaged by two Kodak Megaplus ES1 dual-channel cameras. The size of the measurement region was 4 cm $\times$ 4 cm, and the camera resolution was 0.055 mm/pixel. The angle between each camera and the line perpendicular to the measurement plane was $\theta = 30^{\circ}$. (This angle was limited by the depth of focus of the imaging optics).

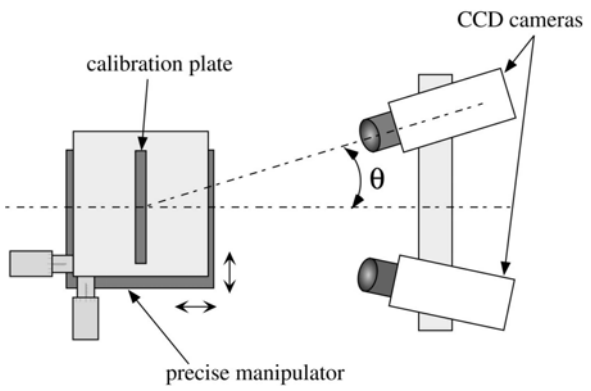

Fig. 3. Set-up for moving plate experiment.

2.3 Jet Flow Experiment

The SPIV system was tested in a two-dimensional oblique jet. The experiments were performed in a vertical Plexiglas water tank with dimensions 10 cm×10 cm×40 cm that was connected to a closed-loop flow circuit (see Fig. 4). Flow entered the tank through a porous round pipe at the upstream end and passed through a number of grids for flow conditioning. The flow then moved through a contoured contraction with area ratio of 3.3 to 1. The width of the contraction outlet t was 3 cm. The mean outlet velocity was 6.0 cm/s with a flow angle of 30° from vertical. The resulting jet Reynolds number was 1800. In all cases, the entire flow was seeded with neutrally buoyant polystyrene particles with diameters ranging from 3-30 microns.

Vertical sheets of flow were illuminated by two frequency-doubled Nd:YAG lasers. The thickness of each sheet was estimated as 1.5-2 mm. The laser firing and camera triggering were controlled by a custom timing circuit. The two Kodak cameras were set up in the same configuration as in the moving plate experiment. Pairs of images captured by the cameras were downloaded to a PC for processing.

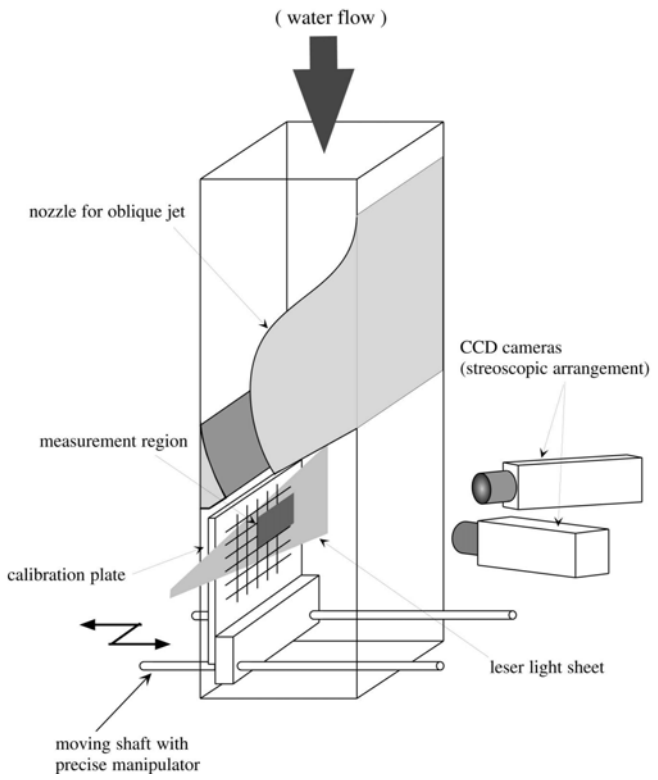

Fig. 4. Jet flow facility and SPIV set-up.

To calibrate the SPIV system in situ, a calibration plate with grid was set up inside of the flow tank. Again, the plate position was controlled precisely with micrometers, and three measurement planes spaced at 0 mm and $\pm$ 4 mm were used to determine the appropriate transform matrices. The plate and traversing system were removed from the facility before flow measurements were conducted. The SPIV measurements were taken in a vertical plane parallel with the jet span.

For comparison purposes, two-dimensional 'classical' PIV measurements were performed in vertical planes normal with the jet span (see Fig. 5). In this case, the same lasers were used in combination with a single Megaplus camera. The measurement plane intersected the central axis of the SPIV measurement plane. In all PIV and SPIV measurements, the time between laser pulses was 10 ms. This resulted in typical tracer particle displacements on the order of 550 microns in the streamwise (y) direction and 230 microns in the normal (z) direction. Interrogation windows were 18 pixels on a side corresponding to 0.83 mm in the measurement plane.

Finally, LDV measurements were performed to obtain time-averaged 'point' velocity statistics in the streamwise (y) and normal (z) directions. A single-component system used the 632.8 nm wavelength from a helium-neon laser. The beam crossing angle was 9.2 degrees yielding a measuring volume of length 1.5 mm and diameter 0.12 mm. The measuring volume length was aligned with the spanwise (x) direction. Collected light was fed to a photomultiplier, and the resulting electronic signals were processed with a digital signal processor attached to a personal computer. Mean and rms velocities were computed from sets of 10000 measurements (y direction) and 6000 measurements (z direction) at each point.

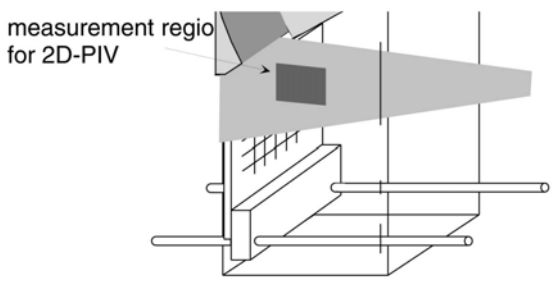

Fig. 5. Set-up for two-dimensional PIV measurements.

3. Results

In all results discussed, the coordinate system is referenced to the stereo PIV set up. The x and y coordinates, which are horizontal and vertical respectively, lie in the plane of the vertical laser sheet, and the z coordinate is perpendicular to the laser sheet.

Figures 6 and 7 show the bias and rms errors determined from the moving plate experiment. In the uppermost plot in Fig. 6, for example, a given 'curve' represents a given x displacement measured at different z displacements. Each data point results from an ensemble average of 1600 displacements calculated from the grid. The plots in Fig. 6 show that the bias errors in the x and y directions were negligible, while the bias in the z direction was fairly constant at about 35 microns (0.6 pixels). The z bias is believed to be caused by calibration limitations, i.e. only three planes encompassing a relatively small depth were used, and quantization error may be a factor.

The plots of rms error in Fig. 7 show the following consistent trend: the error is minimized for zero displacement and increases with increasing displacement in any coordinate direction. This result can be expected based on the idea that the calibration is optimized for zero displacement. The rms error in x is typically small, increasing from 6 microns near the $z = 0$ (or central calibration) plane to 8 microns near z = 2 mm. (5.5 microns = 0.1 pixel). In the y direction, the rms error increases from negligible values near the $z = 0$ plane to values near 20 microns for $z = 2$ mm. Since the y measurement is based on small angles with larger relative uncertainties than the x measurement, a higher uncertainty in y is expected. Nevertheless, in flow experiments, z displacements should normally be limited to about 0.7 mm because of the finite thickness of the laser sheet (refer to Prasad and Adrian, 1993). (In the jet experiment described below, the maximum displacements in z were on the order of 0.3 mm.) For

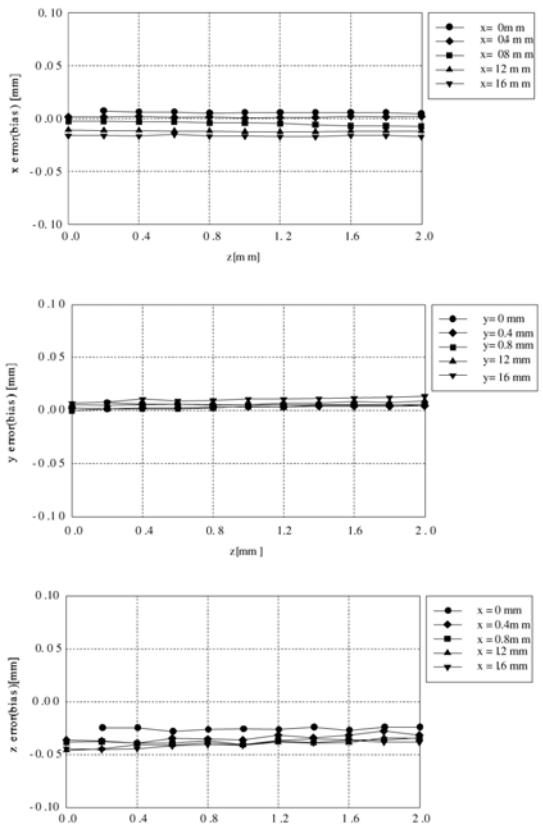

Fig. 6. Bias errors in measured *x*, *y*, *z* displacement.

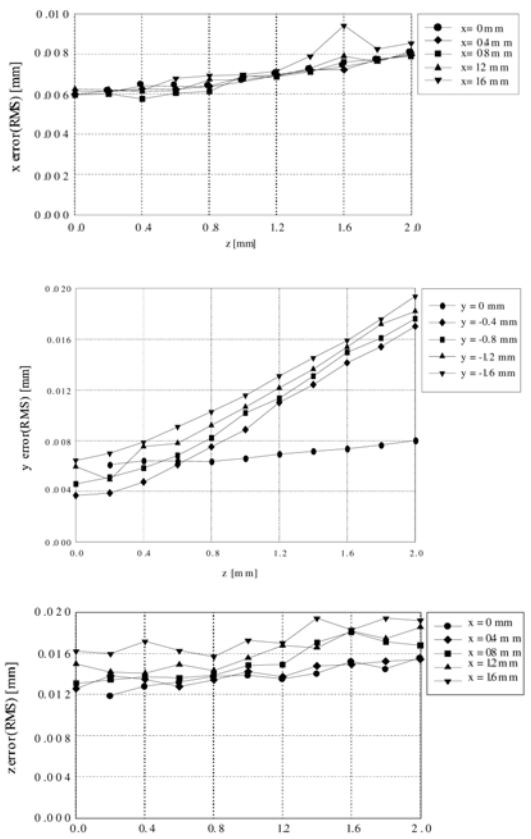

Fig. 7. RMS errors in measured *x*, *y*, *z* displacement.

small *z* displacements, maximum rms errors in *y* displacement are only about 8 microns.

Because the calculated z displacements are dependent on both *x* and *y* values in the recombination process, the rms errors in *z* are largest. These values vary from 12 to 18 microns depending on specific *x* and *z* displacements. The relatively large rms error in the *z* direction is consistent with the results of other researchers such as Soloff, Adrian, and Liu (1997), and likewise is at least partly caused by the limited depth of the calibration domain.

Figure 8 shows an instantaneous velocity field obtained with the classical PIV technique. The position $y = 0$ is located 10 mm downstream of the center of the nozzle exit plane. In this and the subsequent plots, the interrogation regions are not overlapped. Because of the contraction upstream of the nozzle exit, the shear layers of the developing jet are initially small, and the velocity is fairly uniform across the width. Note the two eddies in the shear layer below the jet which have a spacing of about $0.57\boldsymbol{t}$. The shaded section in the figure is centered on the SPIV measurement plane used to generate the plots in Figs. 10 and 11. This plane was chosen in order to capture regions of both low and high mean velocity.

Examples of three SPIV vector maps taken in sequence are shown in Fig. 9. In this sequence, the *z* position has been shifted to the left (compared with Fig. 8) in order to highlight the eddies present in the shear layer below the jet core. The time between plots is 0.33 seconds. These fields indicate that the eddies in the shear layer are in fact three-dimensional, and that the eddies sometimes cause non-uniformities extending into the jet core. Also, the flow pattern toward the outside of the shear layer is strongly three dimensional with streamwise length scales (spacing) on the order of $0.6\boldsymbol{t}$.

Mean and rms velocity statistics were computed from ensemble averages of both classical and stereo PIV measurements, and the results are plotted in Figs. 10 and 11. The PIV measurements are compared with LDV measurements taken separately. The 'classical' measurements were extracted from the shaded area in Fig. 8. Results from 1200 pairs of fields were averaged at *y* positions ranging from 0-40 mm. The SPIV measurements were averaged over a range in the *x* direction of 12.88 mm, assuming that the mean flow was two-dimensional over this section (Stereo PIV 1 in Figs. 10 and 11). Again, 1200 image pairs were used. The two-dimensionality of the mean flow was tested by comparing the data shown with results from a smaller number of total measurements

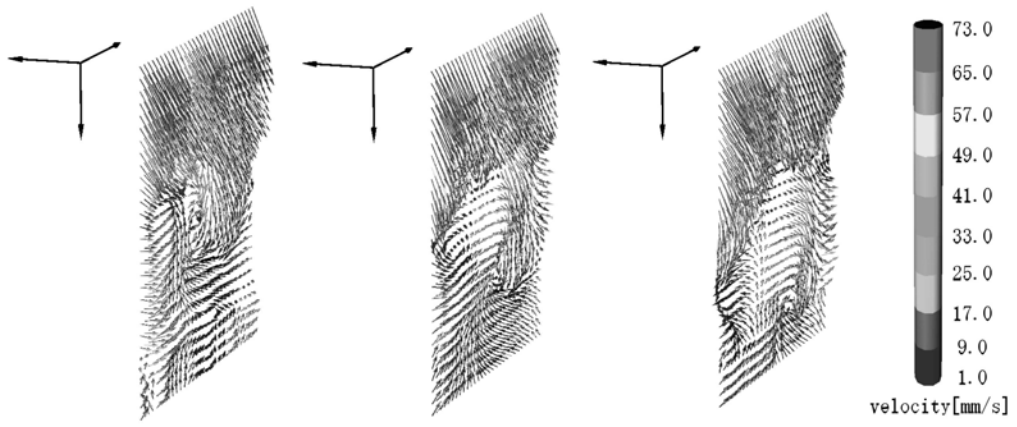

Fig. 8. Instantaneous velocity field obtained by two-dimensional PIV.

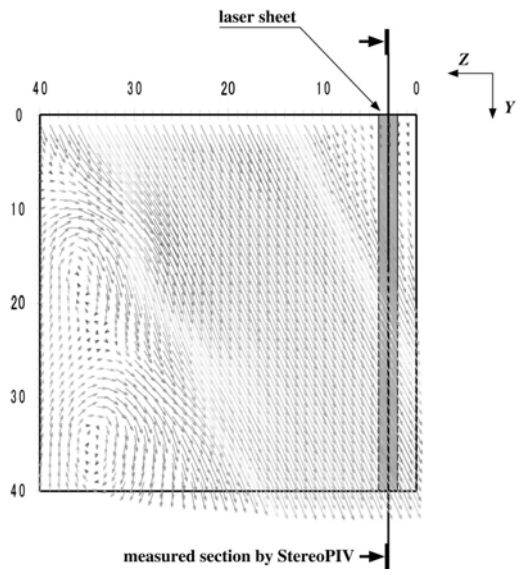

Fig. 9. Sequence of SPIV velocity fields in (x, y) plane.

averaged over a range of 2 mm in the x direction (Stereo PIV 2 in Figs. 10 and 11). The comparison revealed no significant differences in the mean velocity profiles.

The mean velocity plots in Fig. 10 show that the SPIV measurements closely match the classical PIV and LDV measurements in the streamwise (y) direction over the full range in vertical position. In the z direction, the mean SPIV values are slightly lower than the classical PIV and LDV values, especially in the jet core region. If the LDV measurements are assumed correct, then the SPIV measurements are underestimated by about 2.7 mm/s corresponding to a displacement of 27 microns or 0.6 pixels. The systematic difference observed most likely results from a bias error and is consistent with the z bias from the moving plate measurements (Fig. 6).

In Fig. 11, the rms value of the vertical component (v) is similar for the LDV and SPIV methods across the range examined. The classical PIV values are too high where the mean velocity is small. This occurs because of the locally strong mean velocity gradient in the streamwise (y) and wall-normal (z) directions combined with the depth (in z) of the classical PIV measurement region. At a given y position, there is strong variation in the mean velocity with z. This variation causes the exaggerated rms values observed.

In the normal (z) direction, the SPIV rms values match well with the LDV values for $0 < y < 22$ mm. For larger values of y, the SPIV values increase steadily, unlike the LDV values. This is an indication that the rms

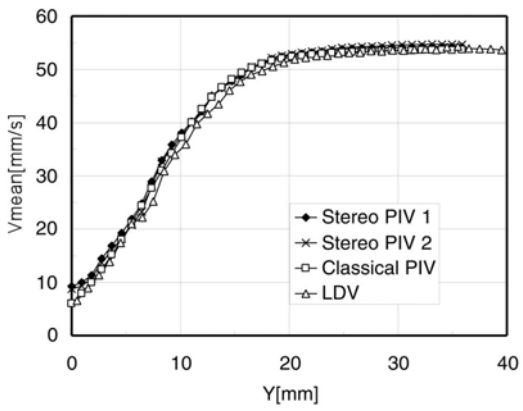

Fig. 10. Ensemble-average mean velocities.

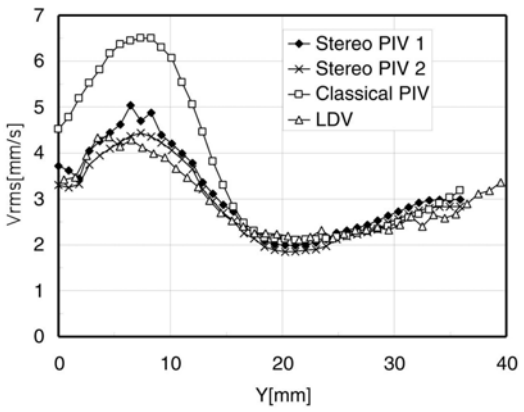

Fig. 11. Ensemble-average rms velocities.

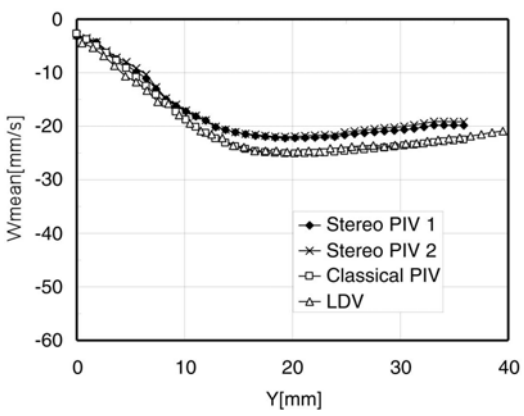

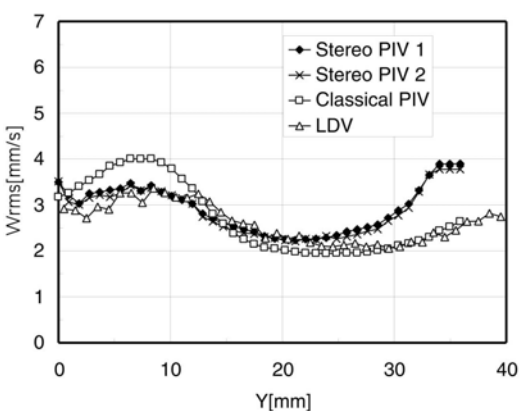

error in the z component of the SPIV calculation increases with increasing y distance from the center of the cameras' field of view. The trend observed is consistent with the increasing rms error in y for increasing magnitude of the y position. (The rms error in z is dependent on the rms error in y). This error would tend to broaden the real velocity distribution and hence increase the rms value measured. In this zone of the flow (where mean gradients are weak in all directions), the classical PIV measurements match the LDV measurements. Note that the LDV measurements yield larger rms values in the streamwise direction than in the wall normal direction (w) in the low speed region of the shear layer. In the jet core, the ratio v_{rms}/w_{rms} is slightly larger than one.

4. Conclusions and Future Work

A stereo PIV system was assembled, tested, and implemented in a relatively simple flow case. The system was found to produce reliable and accurate measurements for mean in-plane velocity when compared with classical PIV and LDV measurements. The out-of-plane mean velocity was underestimated due to bias error in the calibration. In addition, the system performed well at reproducing LDV values for in-plane and some out-of-plane rms measurements. In part of the measurement plane, however, the SPIV system yielded 'rms velocity fluctuations' that were too high. This occurred because of the relatively large rms errors associated with the normal direction in this zone. To remedy the difficulties in measuring 'normal' mean and rms velocities, the SPIV system will be tested in the future with more sophisticated calibration schemes. First, the order of accuracy in determining the normal velocity component will be increased by incorporating z positions into the original mapping matrix similar to the scheme of Soloff et al. (1997). This will eliminate the current approximation that the tail of each vector is centered on the z_0 plane and the effective averaging over the calibration thickness used in determining the vector head. Second, the calibration procedure will be modified to incorporate more than three planes in z and more than one plane inside of the laser sheet thickness. We expect that the higher order calibration schemes will result in decreased uncertainties and distortion errors throughout the measurement field (see Soloff et al., 1997, and Bjorkquist, 1998).

Acknowledgments

Ellen Longmire acknowledges support from NSF (CTS-9457014) and the Tokyo Electric Power Company during a two-month stay at Keio University. The work was also subsidized by the Grant-in Aid of the Japanese Ministry of Education, Science and Culture (No. 10555062). The authors wish to thank Tomotsune Nishimura for help with facility construction and measurements.

References

Abe, M., Stereoscopic and multi-layer PIV system for three-dimensional flow field measurement, M.S. Thesis, Keio University, (1999).

Abe, M., Longmire, E. K., Hishida, K., and Maeda, M., A comparison of 2D and 3D PIV measurements in an Oblique Jet, Proceedings of the Third International Workshop on Particle Image Velocimetry, Santa Barbara, (1999).

Bjorkquist, D. C., Design and calibration of a stereoscopic PIV system, Proceedings of the Ninth International Symposium on Applications of Laser Techniques to Fluid Mechanics, Lisbon, (1998).

Prasad, A. K. and Adrian, R. J., Stereoscopic particle image velocimetry applied to liquid flows, Experiments in Fluids, 15 (1993), 49-60.

Soloff, S. M., Adrian, R. J. and Liu, Z. C., Distortion compensation for generalized stereoscopic particle image velocimetry, Measurement Science & Technology, 8 (1997), 1441-1454.

Willert, C., Stereoscopic digital particle image velocimetry for application in wind tunnel flows, Measurement Science & Technology, 8 (1997), 1465-1479.

Author Profile

Motoyuki Abe: He received M.S. (1999) degrees in engineering from Keio University where he specialized in experimental fluid mechanics and development of fluid measurement devices. Since 1999, he has worked for Hitachi, Ltd. where he is currently research staff in the Mechanical Engineering Research Laboratory. His current research includes studies of fuel injection control for internal combustion engine and development of fuel injector.

Ellen Longmire: She received M.S. (1985) and Ph.D. (1991) degrees in mechanical engineering from Stanford University where she specialized in experimental fluid mechanics. Since 1990, she has taught and directed research at the University of Minnesota where she is currently Associate Professor and Director of Graduate Studies in the Department of Aerospace Engineering and Mechanics. Her current research includes studies of turbulent particle-laden flows, structural identification in turbulence, topological transitions in liquid/liquid mixtures, fluid/structure interactions in microscale flows, and development of flow diagnostics.

Koichi Hishida: He received M.S.(1978) and PhD(1982) degrees in the department of Mechanical Engineering , Keio University. He has researched on heat transfer enhancement in mist flow and turbulent structure in dispersed two-phase flow, and developed dynamic flow measurements based on Laser techniques such as Laser Doppler Velocimetry with particle sizing. He is currently Professor (1997) in the Department of System Design Engineering, Keio University. His current research includes turbulent modification of two-phase flow (particle laden and bubble flows), heat transfer controlling, development of laser based instrumentation for dynamic flow measurements.

Masanobu Maeda: He received M.S.(1962) and PhD(1970) degrees in the department of Mechanical Engineering, Keio University. He worked on Optical Visualization and Measurement of Flow Rate Change with Vena Contracta in a Transonic Channel Flow at the Aerodynamisches Institut of RWTH Aachen as a DAAD scholarship student (1963-1965). Assistant Professor (1976) and Full Professor (1983) in the Department of Mechanical Engineering of Keio University, Yokohama Japan. His research field is emphasized in the experimental analyses of two-phase flow transport phenomena, especially with development and improvement of sophisticated laser techniques.